Journal of Controlled Release 334 (2021) 188–200

Contents lists available at ScienceDirect

Journal of Controlled Release

journal homepage: www.elsevier.com/locate/jconrel

In Vivo bone tissue induction by freeze-dried collagen-nanohydroxyapatite matrix loaded with BMP2/NS1 mRNAs lipopolyplexes

Pinpin Wang [a,f], Federico Perche [a], Patrick Midoux [a], Cátia S.D. Cabral [d], Virginie Malard [a], Ilídio J. Correia [d,e], Hanane EI-Hafci [c], Hervé Petite [c], Delphine Logeart-Avramoglou [c], Chantal Pichon [a,b,*]

[a] Center for Molecular Biophysics (CBM), UPR 4301 CNRS, Orléans, France
[b] Faculty of Science and Techniques, University of Orléans, Orléans, France
[c] Université de Paris, CNRS UMR 7052, INSERM U1271, B3OA, Paris, France
[d] Centro de Investigação em Ciências da Saúde (CICS), Universidade da Beira Interior, Covilha, Portugal
[e] Departamento Engenharia Química, Universidade de Coimbra, Coimbra, Portugal
[f] Shenzhen Institute of Advanced Technology, Chinese Academy Sciences, Shenzhen, China

ARTICLE INFO

Keywords:
mRNA delivery
BMP2
NS1
Collagen-nanohydroxyapatite scaffold
Lipopolyplex
de novo bone formation

ABSTRACT

Messenger RNA (mRNA) activated matrices (RAMs) are interesting to orchestrate tissue and organ regeneration due to the *in-situ* and sustained production of functional proteins. However, the immunogenicity of *in vitro* transcribed mRNA and the paucity of proper *in vivo* mRNA delivery vector need to be overcome to exert the therapeutic potential of RAM. We developed a dual mRNAs system for *in vitro* osteogenesis by co-delivering NS1 mRNA with BMP2 mRNA to inhibit RNA sensors and enhance BMP-2 expression. Next, we evaluated a lipopolyplex (LPR) formulation platform for *in vivo* mRNA delivery and adapted the LPRs for RAM preparation. The LPR formulated BMP2/NS1 mRNAs were incorporated into an optimized collagen-nanohydroxyapatite scaffold and freeze-dried to prepare ready-to-use RAMs. The loaded BMP2/NS1 mRNAs lipopolyplexes maintained their spherical morphology in the RAM, thanks to the core-shell structure of LPR. The mRNAs release from RAMs lasted for 16 days resulting in an enhanced prolonged transgene expression period compared to direct cell transfection. Once subcutaneously implanted in mice, the BMP2/NS1 mRNAs LPRs containing RAMs (RAM-BMP2/NS1) induced significant new bone tissue than those without NS1 mRNA, eight weeks post implantation. Overall, our results demonstrate that the BMP2/NS1 dual mRNAs system is suitable for osteogenic engagement, and the freeze-dried RAM-BMP2/NS1 could be promising off-the-shelf products for clinical orthopedic practice.

1. Introduction

Bone tissue engineering (BTE) applications and regenerative strategies aim at improving current clinical practices for repairing large bone defects resulting from trauma, congenital malformations, and surgical resections [1,2]. BTE is a multidisciplinary field of research, combining biology, material science, chemistry and engineering, with an ultimate goal to create bone graft substitutes (BTE grafts) for bone repair and regeneration [1,3]. A classical BTE graft is composed of a biocompatible and biodegradable scaffold for supportive function, combined with bioactive components, such as osteoinductive growth factors and/or stem cell, for induction of osteogenesis and vascularization [4].

Gene therapy is one alternative method of introducing osteoinductive compounds into the body. In this context, use of gene-activated matrices (GAMs) represent a novel and attractive strategy to promote bone repair. This type of BTE graft carries genetic information (*i.e.* pDNA or mRNA, coding osteogenic proteins) instead of traditional recombinant proteins and cells [5]. The GAMs are designed for long-term *in situ* growth factors expression with proper post-translational modifications at physiological tolerated dose. The feasibility of GAMs as a therapeutic for bone defect repair was fist demonstrated by Fang et al.in 1996 [6]. In their study, the GAM contained two-plasmid DNAs encoding bone morphogenetic protein-4 (BMP-4) and parathyroid hormone fragment (PTH1–34: amino acids 1–34). It was implanted into the rat femoral osteotomy gap. The fibroblasts from invaded granulation tissue became transfected and expressed BMP-4 and PTH1–34. Gap

* Corresponding author at: Center for Molecular Biophysics (CBM), UPR 4301 CNRS, Orléans, France.
E-mail address: chantal.pichon@cnrs.fr (C. Pichon).

https://doi.org/10.1016/j.jconrel.2021.04.021
Received 24 November 2020; Received in revised form 18 April 2021; Accepted 20 April 2021
Available online 23 April 2021

bridging was observed as early as 4 weeks post-GAM implantation. In the next decade, more GAMs were developed. They comprised various genes (*e.g.* vascular endothelial growth factor (VEGF), platelet-derived growth factor-B (PDGF), BMP-2) delivered *via* either viral vectors (*e.g.* adenovirus and recombinant adeno-associated virus) or non-viral vectors (*e.g.* polyethyleneimine, SuperFect™ liposome, and calcium phosphate) [7–11].

To avoid the risk of genome integration and low transfection efficiency inherent with pDNA delivery, matrices progressively releasing the osteogenic factors produced from mRNA or colonized by mesenchymal stem cells (MSC) are emerging for neoformation of bone tissue at the implantation site [12,13]. Aliasger K. Salem group introduced *in vitro* transcribed (IVT) mRNA (encoding BMP-2) activated matrices (RAMs) for bone regeneration [14]. In a rat calvaria defect model, the RAM induced 2-fold and 4-fold more bone tissue when compared to GAM-pDNA (encoding BMP-2) and empty controls, respectively. These encouraging *in vivo* outcomes have been followed by other studies based on RAM containing chemically modified IVT mRNAs [15–17]. The chemical modification is known to suppress IVT mRNA induced immune responses [18]. Despite the advantage obtained using such chemically modified mRNA, the main drawbacks are their high cost and the required tuning of chemical modifications according to gene and cell types [19].

Instead of using chemically modified mRNA, another strategy is to co-express the mRNA of osteogenic genes with the mRNA coding for an immune evasion protein as the influenza A virus derived NS1, known to inhibit type I interferon (IFNα/β) expression, protein kinase R (PKR) and 2′-5′-oligoadenlate synthase (OAS) activation [20,21]. In our previous study, we first demonstrated that co-delivering BMP2 mRNA and NS1 mRNA in murine pluripotent stem cells (C3H10T1/2) was able to promote their osteogenic differentiation *in vitro* [22]. We have established the optimal weight ratio between BMP2 and NS1 mRNAs (3:1). Dual delivery of BMP2 and NS1 mRNA resulted in the inhibition of immune sensors and inflammatory cytokines production and the improved expression of osteogenic markers in comparison to the delivery of BMP2 mRNA alone.

The next step of this work is to assess the potentiality of this strategy *in vivo*, which requires an effective delivery, the other challenge for mRNA therapy besides the immunogenicity issue [23]. We have developed a lipopolyplex (Lip100/His-lPEI/RNA ternary complex, LPR) platform capable of efficient *in vitro* and *in vivo* cell transfection with a negligible toxicity [24,25]. The imidazole/imidazolium binary Lip100 liposomes are made of cationic O,O-dioleyl-N-(3 N-(*N*-methylimidazolium iodide) propylene) phosphoramidate (KLN25) and neutral O,O-dioleyl-N-histamine phosphoramidate (MM27), at a molar ratio of 1:1 [26,27]. KLN25 possesses an *N*-methylimidazolium polar head conferring a permanent positive charge used for nucleic acids condensation. The imidazole group of MM27 is not alkylated on the nitrogen atoms allowing the acquisition of cationic charges at the environmental pH below 6 and favoring the endosome destabilization and nucleic acids release (endosome escape). The cationic polymer His-lPEI, is a histidylated linear polyethyleneimine [28]. As in MM27, the protonation of imidazole groups from histidine increases endosome escape of trapped nucleic acids leading to higher transfection efficiency compared to lPEI [29].

In the present work, we evaluated whether i) the dual mRNA system (BMP2/NS1 mRNAs) is able to promote osteogenesis of human mesenchymal stromal cells (hMSCs); ii), the LPRs platform is suitable for *in vivo* mRNA *in-situ* delivery and iii), BMP2/NS1 mRNAs formulated LPRs can induce new bone tissue formation *in vivo* when combined in suitable matrix.

To this aim, we delivered BMP2/NS1 mRNAs into hMSCs and measured the BMP2 production and hMSCs osteogenic differentiation; we then prepared LPRs with firefly luciferase mRNA and assessed the luciferase production after intradermal administration; next, the BMP2/NS1 mRNAs LPR nanoparticles were formulated and incorporated into collagen-nanohydroxyapatite scaffolds to form mRNA-activated matrices (RAMs). The release and the translation of the mRNA containing LPRs from RAMs were determined *in vitro* and the efficiency of RAMs to induce *de novo* bone formation was evaluated by subcutaneously implanting them into mice back.

2. Materials and methods

2.1. IVT mRNAs preparation

The pT7-GFP [30], pT7-BMP2 and pT7-NS1 [22] plasmids were linearized with either *Spe*I or *Not*I, for mRNAs production with the mMessage mMachine T7 kit (Ambion) according to the manufacturer's instructions. The poly(A) tail was added with PolyA polymerase (Ambion). Synthesized mRNAs were purified with phenol/chloroform and isopropanol precipitation. Purity, size and integrity of the mRNAs were verified by a UV spectrophotometer (NanoDrop One, Thermo Scientific) and denaturing agarose gel electrophoresis, respectively.

2.2. Cell culture

C2C12 cells were purchased from American Type Cell Collection (ATCC), and cultured in Dulbecco's modified eagle media (DMEM, Sigma) containing 10% heat-inactivated fetal bovine serum (FBS; Sigma) and 1% antibiotics (Sigma). C2C12-BRE/Luc cells containing BMP-2 response element (BRE), which express luciferase under BMP-2 stimulation, were previously described [31]. Human MSCs were harvested from bone marrow obtained from discarded tissue during routine bone surgery from 3 donors (1 woman and 2 men; 15, 22, and 31 years old, respectively) at the Lariboisiere Hospital, Paris, France. The tissues were collected with the respective donor's consent in agreement with Lariboisiere Hospital regulations. hMSCs were isolated from each donor's bone marrow using a procedure as previously reported [32,33]. Briefly, hMSCs were harvested by gently flushing the bone marrow using complete growth medium (specifically, alpha-Minimum Essential Medium (α-MEM, PAN Biotech) containing 10% heat-inactivated fetal bovine serum (FBS; Sigma) and 1% antibiotics (Sigma). These cells were characterized by expression of selected CD markers (specifically, positive for CD90, CD73, CD105 and negative for CD45; data not shown). At passage 1, hMSCs from each donor were pooled at an equal ratio, and used for experiments less than passage 8.

All cells were cultured at 37 °C in a humidified atmosphere containing 5% CO_2, and mycoplasma-free as evidenced by MycoAlert Mycoplasma Detection Kit (Lonza).

2.3. Lipopolyplex (LPR) preparation and characterization

The His-lPEI grafted with 16% histidine residues was synthesized as previously described [28], and purchased from Polytheragene SAS (Genepole, Evry, France). KLN25 and MM27 were synthesized as previously described [26,27]. The Lip100 containing an equal molar ratio of KLN25 and MM27 was prepared as previously described [24,34].

Lipopolyplexes were prepared according to [24] with some modifications (Fig. 1A). In brief, 15 μl HEPES (10 mM, pH 7.4) containing 7.5 μg His-lPEI was added into 37.5 μl HEPES (containing 2.5 μg mRNA) under vortex followed by 30 min incubation at RT to allow the polyplexes formation. Then, the polyplexes were added into liposome solution (3 μl 5.4 mM Lip100 in 197 μl HEPES), and pipetted up and down for 5 times followed by 15 min incubation at RT, allowing the LPRs formation.

2.3.1. LPR particle size, zeta potential and mRNA encapsulation

LPR particle size and zeta potential were measured in 10 mM Hepes buffer, pH 7.4 by dynamic light scattering and electrophoretic mobility using a nanoparticle analyzer SZ-100 (Horiba Scientific).

mRNA encapsulation efficiency of the LPR formulation was

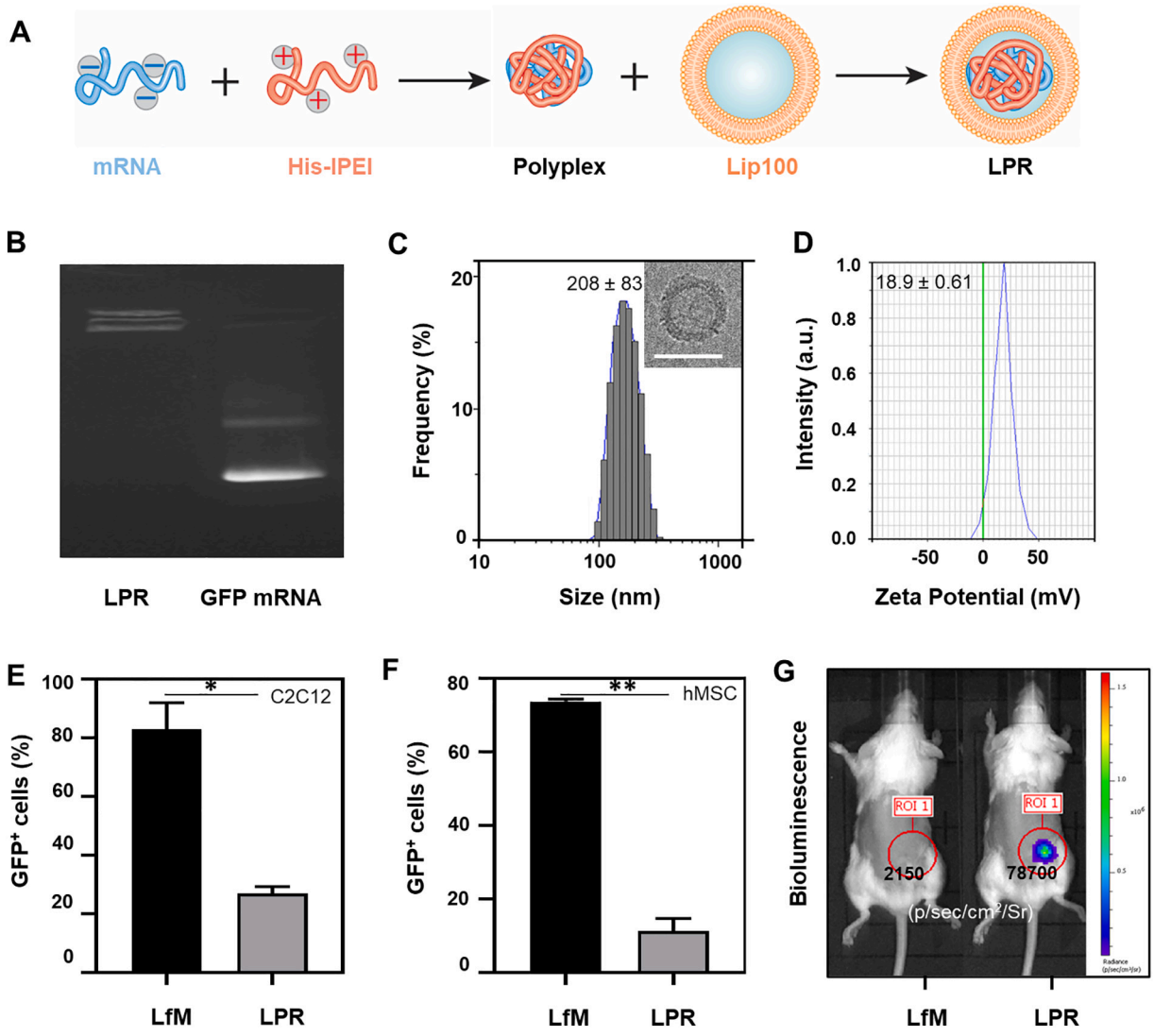

Fig. 1. Lipopolyplexes formulation and transfection efficiency. (A) Illustration of LPR preparation. mRNA was first complexed with His-lPEI to form polyplexes, which are mixed with Lip100 liposomes to form LPR nanoparticles. (B) Agarose gel electrophoresis of LPRs and eGFP mRNA. (C, D) LPR physico-chemical characterization. The representative diagram of LPRs (complexing with eGFP mRNA) hydrodynamic diameter distribution (inset: TEM image of LPR with scale bar = 100 nm), and zeta potential. (E, F) *In vitro* transfection efficiency. hMSC and C2C12 Cells were transfected either with LPRs containing eGFP/NS1 mRNAs (3:1 weight ratio, 2.5 μg mRNA in total) or with Lipofectamine Messengermax (LfM) containing the same mRNAs content. 24 h post-transfection, the eGFP positive population was quantified *via* flow cytometry. *t*-test was used for statistical analysis. (G) *In vivo* transfection efficiency. LPRs or LfM formulations comprising firefly luciferase mRNA and NS1 mRNA (3:1, weight ratio, 5 μg in total) were intradermally injected. One-day post-injection, *in vivo* luciferase expression was observed with IVIS Lumina LT *In Vivo* Imaging System.

measured through agarose electrophoresis. LPRs (5 μg Lip100/7.5 μg His-lPEI /2.5 μg eGFP mRNA) and 2.5 μg free eGFP mRNA were run in 1% agarose gel. The mRNA retardation was observed *via* a gel documentation system (GeneFlash, Syngene).

2.3.2. LPR morphology

LPR morphology was analyzed by transmission electron microscopy (TEM) using a Philips CM20/STEM electron microscope operating at 50 kV. TEM samples were prepared according to the technique of negative staining using uranyl acetate as reported by Perche et al., [30]. Five ml LPR solution in HEPES buffer was deposited on a carbon-coated copper grid for 5 min; and then adsorbed with filter paper. 5 ml uranyl acetate 2% in RNase-free water was then, deposited on the grid for 10 s. Samples were dried at room temperature for 20 min before TEM observation.

2.3.3. LPR transfection efficiency

One day before *in vitro* transfection, 1×10^5 C2C12 cells/well were seeded onto 24-well plate. The next day, 1.875 μg GFP/0.625 μg NS1 mRNAs were formulated into LPRs, and delivered to C2C12 cells. Lipofectamine™ MessengerMax (LfM, Invitrogen) complexing same amount of mRNA was set as control. 24 h post-transfection, the GFP expression was quantified by flow cytometry (FACSort, Becton Dickinson).

For *in vivo* transfection, LPRs containing 3.75 μg Fluc/1.25 μg NS1 mRNAs were intradermally injected into mouse skin. LfM/mRNA complexes intradermal injection was set as control. 24 h post-injection, the *in vivo* luciferase expression was observed with IVIS Lumina LT *In Vivo* Imaging System (PerkinElmer). The radiance quantification was done using the Living Image® software (Perkin Elmer) with the same threshold of minimal signal.

2.4. Osteogenic commitment of hMSCs

Lipofectamine™ MessengerMax (LfM) was used for hMSCs

transfection according to the manufacturer's protocol.

2.4.1. Quantification of BMP-2 released by transfected hMSCs

hMSCs were seeded in a 12-well plate at 1×10^5 cells/well. The next day, cells were transfected with either 1 μg BMP2 mRNA or 0.75 μg BMP2 mRNA/0.25 μg NS1. Every 12 h, half culture medium (containing the released BMP-2) was collected and replaced with fresh growth medium. Collected media were stored at −80 °C before BMP-2 quantification. BMP-2 contents were determined by ELISA (Abcam kit) following the manufacturer's instruction. The absorbance was measured at 450 nm (^{3}V spectrophotometer, PerkinElmer) and BMP-2 contents were calculated based on a standard curve (range: 0-4000 pg/ml human BMP-2).

2.4.2. Osteoblastic differentiation assay of transfected hMSCs

5×10^4 hMSCs were seeded into each well of 12-well plate, and cultured in growth medium for one week until confluence. Then, 0.5 μg BMP2 mRNA or 0.325 μg BMP2 mRNA/0.125 μg NS1 mRNA were delivered as lipoplexes to the cells. The cell culture medium was changed to modified osteogenic medium, which consisted of the growth medium plus 10 mM beta-glycerophosphate (β-GP, Sigma) and 150 μM ascorbic acid-2-phosphate (As2P, Sigma).

At day 1, 3, 5, 7, 14, and 21 post-transfection, the gene expressions of Runx2, Alkaline phosphatase (ALP), osteocalcin (OCN), osteopontin (OPN) were quantified by real-time quantitative reverse-transcription polymerase chain reaction (RT-qPCR) according to a previous report [35]. Briefly, total RNA was isolated and purified by TRIzol (Life technology)-chloroform method. RNA concentration and purity were measured using Nanodrop (ThermoFisher). First-strand cDNA synthesis kit (Thermo Scientific) was used for reverse transcription following the manufacturer's protocol. qPCR was performed using the Luna qPCR Master Mix (NEB) with a Light Cycler© 480 PCR system (Roche). The qPCR data were analyzed by the comparative $^{\Delta\Delta}$Ct method using the GAPDH RT-qPCR signal as an internal control for normalization. Primers for RT-qPCR were synthesized by Eurogentec, and the sequences were listed in Supplementary Table 1.

Alizarin Red staining was performed 28 days post-transfection to evaluate the calcium deposition within the extracellular matrix. Cells were washed with DPBS and then fixed in 4% p-formaldehyde for 30 min at room temperature (RT) followed by 2 times washes with distilled water (dH_2O). The extracellular calcium deposits were stained by incubating the cells in Alizarin red S (Sigma) solution (saturated in dH_2O, pH 4.1). Nonspecific staining was removed by washing cell layers with dH_2O five times under gentle agitation. To quantify the mineralization, the alizarin red dye was subsequently extracted with cetylpyridinium chloride (Sigma) solution (10% in 10 mM sodium phosphate) for 30 min at RT. Absorbance was then measured at 560 nm using the Victor ^{3}V spectrophotometer (PerkinElmer).

2.5. Collagen-nanohydroxyapatite scaffolds preparation and characterization

The collagen-nanohydroxyapatite scaffolds (CoLL-nHA) were prepared as reported previously [36,37] with some modifications. Briefly, the collagen (Calf skin type I collagen, MP Biomedicals) was first hydrated in 0.1 M acetic acid overnight at 4 °C. The nano-sized hydroxyapatite (<50 nm, Sigma) was dispersed in 0.1 M acetic acid by applying two runs of sonication, for 30 min each. The hydroxyapatite suspension was then dropped into the collagen slurry under vortexing (final collagen concentration was 0.75% *w/v*). The resultant CoLL-nHA mix was further homogenized overnight at 4 °C using a roller mixer (Cat Ingenieurbuero™ RM540), then degassed under vacuum for 1 min, and dispatched into polypropylene containers. The CoLL-nHA suspension was frozen at −80 °C for 2 h with a cooling rate of 1 °C/min and lyophilized by sublimation at −80 °C and 0.1 mbar for at least 16 h (Bioblock Scientific). The CoLL-nHA scaffolds were then crosslinked by incubating the foams with 1-ethyl-3-(3-dimethylaminopropyl) carbodiimide hydrochloride (EDC) and N-hydroxysuccinimide (NHS) [38] in 95% ethanol at RT for 3 h. The scaffolds were then washed five times in distilled water for 15 min each and freeze-dried by described above.

Three types of scaffold were prepared: collagen scaffold without nHA (CoLL); scaffold containing collagen and nHA at the mass ratio of 1:1 (CoLL-1nHA), and 1:3 (CoLL-3nHA).

2.5.1. Microstructure

The scaffold microstructures were observed with a scanning electron microscope (SEM) (Zeiss Ultra Plus, Carl Zeiss) after mounting on SEM stubs and coating with gold-palladium.

2.5.2. Pore size and porosity

Pore size was measured using the ImageJ software (1.52a, National Institutes of Health) according to previously reported study [39]. Briefly, 50 randomly selected pores from each of 8 SEM images (from two different samples) were analyzed. The circularities were assumed as 1 for pore size calculation.

Porosity was assayed by the liquid displacement method [40,41]. Briefly, the scaffold was immersed in 1 ml (V1) distilled water in a cylindrical container, and a vacuum was applied for 1 min allowing water fully infiltrate into the scaffold. After that, the total volume of water plus scaffold was defined as V2. Then, the water-impregnated scaffold was removed from the container, the remaining water volume was V3 and the porosity was calculated as follows:

Porosity = (V1-V3) / (V2-V3).

2.5.3. Mechanical strength

The mechanical measurements were performed at room temperature using a tensile testing machine (AG-X, Shimadzu) with a crosshead speed of 2 mm/min and a load cell of 5 kN. The compressive strength (Cs) was determined with the following Equation:

$Cs = F/A$.

where F corresponds to the load strength (N) at the time of fracture and A represents the scaffold contact area (mm).

2.5.4. Cytocompatibility

1×10^4 C2C12 cells suspended in 100 μl medium were dropped onto each type of scaffold (cylindrical in shape, 6 mm diameter × 2.5 mm height), and incubated for 2 h to allow cell adhesion, then cultured after addition of culture medium.

Cell proliferation inside the scaffolds was measured with Cell Proliferation Kit II (XTT) (Sigma-Aldrich) according to the manufacturer's instruction with minor modifications. Briefly, at defined time points, cell constructs were washed twice with DPBS with gentle squeezing for complete medium removal. After removing the remnant DPBS with an absorbent tissue, the cell constructs were immerged into the reaction mix (200 μl culture medium, 50 μl XTT solution, and 1 μl electron-coupling reagent) and maintained for 4 h. From each well, 100 μl of solution was transferred into 96-well plate, and the absorbance was read at 450 nm and 650 nm with Victor ^{3}V spectrophotometer (PerkinElmer).

Cell density and morphology were observed with confocal laser scanning microscopy (LSM510, Zeiss). The constructs were washed as described above, and then fixed with methanol (90%) at −20 °C for 30 min; the cells containing constructs were blocked with PBS-1% BSA at RT for 1 h, incubated with anti-actin antibody (Sigma) at RT for 2 h; after washing, the constructs were incubated with Alexa Fluor® 488 conjugated secondary antibody (Invitrogen) at RT for 2 h before observation.

2.6. mRNA activated matrices (RAMs) preparation and characterization

The LPRs were prepared as described above, except that the total volume was decreased 10-fold and containing 5% sucrose. Concentrated LPRs containing 20 μg mRNA were loaded into each CoLL-1nHA scaffold

disc (6 mm × 2.5 mm), which were then freeze-dried. The mRNA activated matrices (RAMs) were stored at −20 °C for further usage.

The SEM observation and mechanical test of RAMs were performed as described in Section 2.3.1 and 2.3.3.

2.6.1. LPRs release kinetics. The RAMs were immerged in 1 ml RNase-free TE buffer (10 mM Tris-HCl, 1 mM EDTA, pH 7.5) and incubated at 37 °C. At scheduled time points, 800 μl TE buffer was collected and replaced with fresh RNase-free TE buffer. All collected samples were stored at −80 °C for further measurement. The released LPRs were labeled with Quant-iT™ RiboGreen (Invitrogen) following the manufacturer's instruction, and then quantified by a spectrophotometer (excitation: 490 nm; emission: 525 nm) (Victor ^{3}V, PerkinElmer).

2.6.2. In vitro LPRs release and transfection. 1×10^5 C2C12-BRE/Luc cells were seeded into each well of 24-well plate. The next day, RAMs either containing 20 μg BMP2 mRNA (RAM-BMP2) or 15 μg BMP2/ 5 μg NS1 mRNAs (RAM-BMP2/NS1) were added into each well. At the defined time points, cells were lysed (RIPA, Thermofisher) and stored at −80 °C. Luciferase activity was measured as previously reported [34]. Cells transfected with fresh prepared LPRs containing 1 μg BMP2 mRNA or 0.75 μg BMP2/0.25 μg NS1 mRNAs were set as control.

2.7. In vivo de novo osteogenesis

2.7.1. In vivo implantation

The osteoinductive potential of scaffolds was assessed *in vivo* in a mouse ectopic model. Four-week-old, male, BALB/c mice were purchased from Janvier, and handled in accordance with the European Directive 2010/63/EU regarding the protection of animals used for scientific purposes. All animal experiments were performed with the approval of the French ministry of research (approval number: 15910–2,020,030,213,573,920). The RAM-BMP2 and RAM-BMP2/NS1 were subcutaneously implanted into mice back as previously described [42] (one RAM per mouse, $n = 8$ per group). Empty CoLL-1nHA scaffolds were used as control ($n = 3$). Eight weeks post-implantation, the mice were sacrificed through cervical dislocation. The RAMs were excised and fixed in 4% paraformaldehyde.

2.7.2. Micro-computed tomography (μCT) analysis

The new bone formation induced by the BMP-2-expressing RAMs was determined by μ-CT analysis using a Skyscan 1172 high resolution μ-CT scanner (Bruker). Images were acquired using the following settings: voltage 80 kV, current 100 μA, exposure for 810 ms, and 0.4-degree rotation-step settings, through a 0.5 mm-thick aluminium filter. The initial pixel size at these settings was 6 μm. The scanned images of each implant were reconstructed as a stack of slices using Nrecon software (Bruker). The new bone volume per each scaffold was determined using the CTAn software (v1.15.4.0; Bruker; grayscale threshold values within 123–240). The binarization threshold was determined by Otsu's method, based on histograms of 3D μCT scans of bone containing scaffolds.

2.7.3. Histological analysis

Retrieved implants were processed for decalcified histology. Samples were decalcified in ethylenediaminetetraacetic acid (14.5% *w/v*) at 4 °C for 2 weeks, and embedded in paraffin. Some sequential sections of each specimen were stained with Masson's Trichrome and TRAP staining.

2.8. Statistical analysis

Unless otherwise indicated, the numerical data are expressed as mean ± standard deviation with $n = 3$. Statistical analysis was performed using GraphPad Prism version 6.07 (GraphPad software). Any *p*-value less than 0.05 was considered statistically significant. Specifically, * represents $P < 0.05$; ** represents $P < 0.01$; *** represents $P < 0.001$; **** represents $P < 0.0001$.

3. Results

3.1. LPR generates higher in vivo mRNA delivery efficacy than in vitro

To efficiently deliver BMP2 and NS1 mRNAs, we compared LPR formulation with a commercial vector Lipofectamine™ MessengerMax (LfM). LPR formulation was prepared by a well-established two-step approach. First, mRNA was complexed with His-lPEI (1/3, mRNA/His-lPEI weight ratio), and the resulting polyplexes were mixed with Lip100 liposomes (1/2, mRNA/Lip100 weight ratio) [24,34] (Fig. 1A). The agarose gel electrophoretic mobility shift assay, in which no free mRNA migration was observed (Fig. 1B), confirmed the complexation of mRNA. The LPRs had a mean hydrodynamic diameter of 208 nm with the core morphology of mRNA/His-lPEI complex surrounded by the lipid bilayer structure of Lip100 liposome (Fig. 1C-insert). The mean zeta potential of LPRs were slightly positively charged (+ 18.9 ± 0.6 mV) as shown in Fig. 1D.

As the main goal of our study was to evaluate the efficiency of our strategy for *de novo* bone formation following subcutaneous implantation of RAM and myoblasts from back muscle could be one of the sources of cells that can colonize the implanted scaffold, we checked their ability of LPR to transfect murine C2C12 cells, a myoblast cell line. As shown in Fig. 1E, LPRs transfection resulted in only 27% of transfected cells whilst LfM led to 83% of positive cells. For clinical relevance, hMSC transfection was performed as well. Similarly, LPRs yielded 9% transfection efficiency which was 73% for LfM (Fig. 1F). However, the trend was completely reversed *in vivo* following intradermal injection, a strong bioluminescence around the injection site was observed following LPRs injection, while, no detectable signal was found on the site injected with LfM/mRNA complexes (Fig. 1G).

3.2. BMP2/NS1 mRNAs delivery favors hMSC osteogenic commitment

Before evaluating the efficiency of our strategy for RAMs implantation *in vivo*, we first sought to assess whether the delivery of BMP2 mRNA and NS1 mRNA is also able to enhance BMP-2 production in human mesenchymal stem cells. For those experiments, we used LfM as commercial standard for the mRNA delivery. We performed the transfection at the BMP2: NS1 mass ratio of 3:1 based on our previous study [22]. The BMP-2 content was quantified in culture media collected every 12 h (Fig. 2A). Compared to the transfection of BMP2 mRNA alone, co-transfection with NS1 mRNA increased significantly the BMP-2 production from the early (12 h–24 h) to the later (48 h–60 h) time points. Following BMP2/NS1 mRNAs transfection, the peak of BMP-2 production started at 24 h and maintained up to 36 h. The BMP-2 expression steadily increased up to 36 h. By contrast, following the transfection of BMP-2 mRNA alone, the maximal BMP-2 content was obtained in the first 12 h, and then decreased as a function of time. These data confirm that the platform is potentially translatable in human context at least concerning the ratio between the mRNA of the osteogenic gene and that of NS1.

The osteogenic differentiation of hMSCs was evaluated by quantifying osteogenesis-related gene expression and extracellular matrix (ECM) mineralization (Fig. 2B—D). On day 1, 3, 7, 14 and 21 post-transfection, transcripts were quantified by RT-qPCR (Fig. 2B). Throughout the measuring time, the Runx2, ALP, OPN and OCN expression in BMP2/NS1 group was higher than that in BMP2 group. However, no significant differences were found, excepted for Runx2 expression on day 3. Both Runx2, OPN and OCN shown a two stages expression profile with different peaking times, *i.e.*, day 3 for Runx2, day 7 for OPN, and day 3 for OCN. Interesting, ALP expression peaked on day

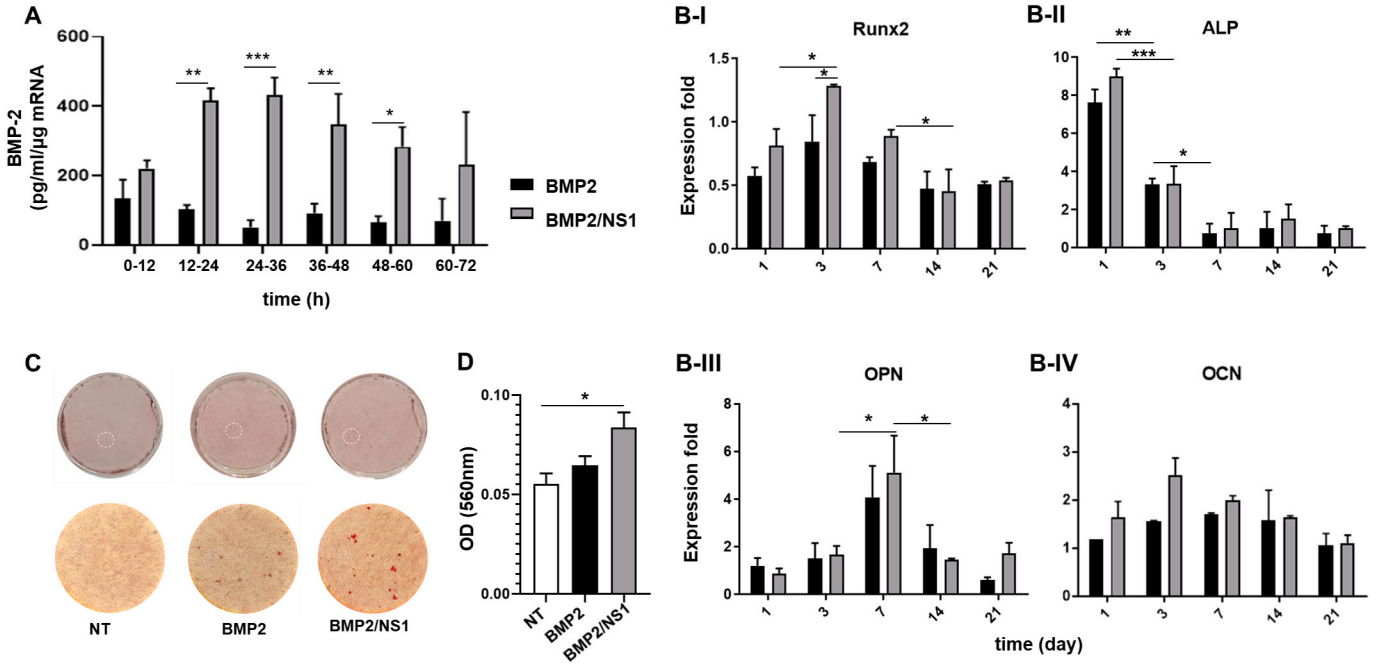

Fig. 2. hMSCs osteogenic commitment. (A) The secreted BMP-2 from hMSCs transfected with either 1 μg BMP2 mRNA (BMP2) or 0.75 μg BMP2/0.25 μg NS1 mRNAs. Secreted BMP-2 was quantified by ELISA every 12 h post-transfection. 2way ANOVA, Sidak's multiple comparisons test, was used for statistical analysis. (B) The expression of transcripts of osteoblastic genes was measured at day 1, day 3, day 7, day 14 and day 21 post-transfection by RT-qPCR, and normalized to non-treated cells (NT). 2ˆ-ΔΔCt method was used in the calculation. 2way ANOVA, Tukey's multiple comparisons test, was used for statistical analysis. (C) The calcification of extracellular matrix (ECM) was observed *via* ARS staining, 28 days post-transfection. Top, photographs of wells; bottom, micrographs (10×) taken from the above white circles indicated areas. (D) The extracellular calcium was quantified by dissolving the ARS-aggregates into 10% cetylpyridinium chloride (CPC) followed by an optical density (OD) assay at 560 nm. Ordinary one-way ANOVA, Tukey's multiple comparisons test, was used for statistical analysis.

1 post-transfection, and sharply decreased on day 3. Twenty-eight days post-transfection, the deposited calcium was stained with Alizarin Red S (ARS) and quantified (Fig. 2C, D). Compared to the NT group and BMP2 group, the BMP2/NS1 group showed more calcium nodules. Quantification results, by dissolving the ARS staining in 10% cetylpyridinium chloride solution, demonstrate that the BMP2/NS1 mRNAs delivery induced significantly higher calcium deposition than NT group, while the BMP2 mRNA delivery did not.

3.3. *nanoHydroxyapatite reinforces collagen matrix*

In a view of producing RAMs, we decided to prepare biomimetic collagen-based scaffolds that bear different percentage of nano-hydroxyapatite, the main inorganic bone component. Three types of collagen-based scaffolds with collagen/nanohydroxyapatite weight ratio of either 1/0 (CoLL), 1/1 (CoLL-1nHA) or 1/3 (CoLL-3nHA) were produced by a freeze-drying approach using acetic acid as a porogen. The scanning electron microscopy was performed to observe their porous structure (Fig. 3A). CoLL (Fig. 3A-a) and CoLL-1nHA (Fig. 3A-c) exhibited similar microstructure with connected macro- (>100 μm) and micro-pores (<50 μm), whilst CoLL-3nHA (Fig. 3A-e) was denser and devoid of micropores. The SEM images observed under the high magnification revealed embedded nHA particles (Fig. 3A-d and f). Two key parameters, *i.e.* pore size and porosity, of porous scaffold were quantified. As shown in Fig. 3B and C, CoLL, CoLL-1nHA and CoLL-3nHA had an average pore size/porosity of 168.7 μm/ 91.26%, 151 μm/ 89% and 165.9 μm/ 76%, respectively. Compared to CoLL, both CoLL-1nHA and CoLL-3nHA demonstrated higher compressive strength in axial and radial orientations (Fig. 3D). The differences between CoLL and CoLL-3nHA are significant.

The cytocompatibility of the three collagen-based scaffolds was evaluated by seeding C2C12 cells (Fig. 4A). One day after cell seeding, XTT assay results reveal that more cells were attached to CoLL-1nHA compared to CoLL-3nHA and CoLL. The OD values significantly increased from day 1 to day 3 and remained steady at day 7, indicating that the cells were proliferating within the scaffolds during the first 3 days post-seeding followed by a stagnation. No significant differences in cell viability were observed among each type of scaffold tested. Actin filaments of cells were labeled to visualize the cell distribution within the CoLL-1nHA scaffold (Fig. 4B). At day 1, faint labeling corresponding to few dispersed cells were observed in the scaffold matrix. One week later, one can observe a dense cellular network filling the field.

3.4. *LPRs resistant to freeze-drying*

To produce RAM, LPRs or LfM/mRNA complexes containing 20 μg mRNA were dropped onto CoLL-1nHA and then freeze-dried (Fig. 5B-insert). We performed scanning Electron Microscopy (SEM) experiments to visualize the structure of RAM and vector/mRNA nanoparticles in RAM. The SEM images show the two RAMs had similar porous structure (Fig. 5A-top and B-top), but strongly differed in the morphology of vector/mRNA complexes. Whereas LPRs maintained their spherical morphology (Fig. 5B-bottom), the LfM/mRNA nanoparticles broke and collapsed (Fig. 5A-bottom).

The LPRs loading did not impact the average pore size of CoLL-1nHA (Fig. 5C), while increased its mechanical strength (Fig. 5D). Compared to CoLL-1nHA, the axial compressive strength and radial compressive strength of RAM increased 6.3-fold and 1.7-fold, respectively.

3.5. *RAM serves as LPRs release platform*

The loading efficiency and release kinetics of LPRs from RAM were then evaluated (Fig. 6. A). The quantification of unloaded LPRs, which leaked into the container during RAM preparation revealed that 74% LPRs were absorbed by the CoLL-1nHA scaffold. The release of LPRs from RAMs was monitored along time. The kinetics showed a fast release

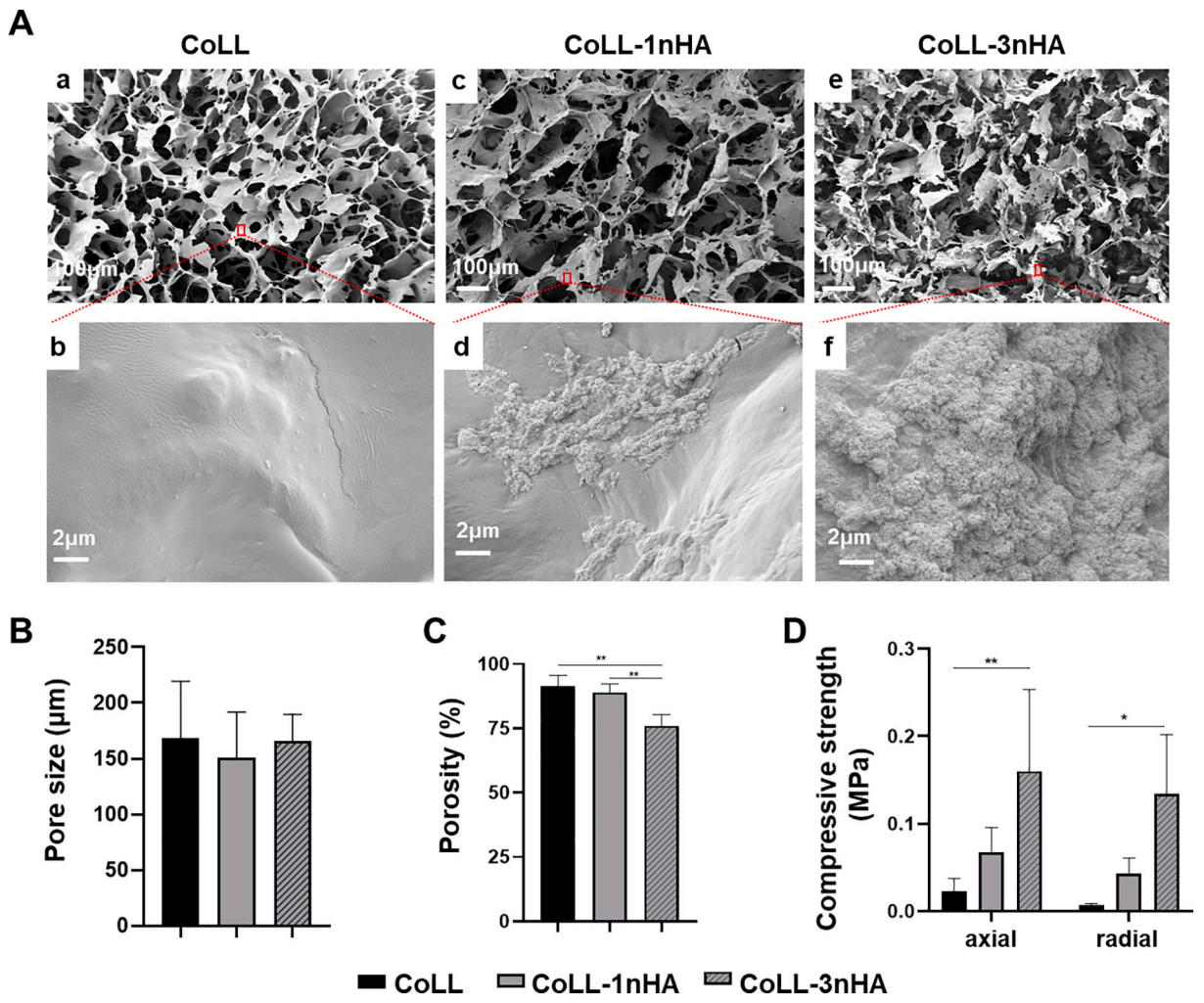

Fig. 3. Characterization of collagen and collagen-nanohydroxyapatite scaffolds. (A) The representative SEM images of collagen scaffold (CoLL: a, b), collagen-nanohydroxyapatite scaffold with 1: 1 mass ratio of collagen to nanohydroxyapatite (CoLL-1nHA: c, d), and 1: 3 mass ratio of collagen to nanohydroxyapatite (CoLL-3nHA: e, f). $n = 4$. (B) Relative measurement of CoLL, CoLL-1nHA and CoLL-3nHA pore sizes, calculated by ImageJ software based on SEM images ($n = 8$). (C) The open porosities of CoLL, CoLL-1nHA and CoLL-3nHA calculated by the liquid displacement method (n = 4). Ordinary one-way ANOVA, Tukey's multiple comparisons test, was applied for statistical analysis. (D) The scaffolds' compressive strength. The axial and radial mechanical performances of the three types of scaffold (n = 4). Statistical analysis was calculated with 2way ANOVA, Tukey's multiple comparisons test.

in the first 120 h (37% of loaded LPRs) followed by a slow release ending up to 46% afterwards (Fig. 6. B). In order to assess the activity of released LPRs, the BMP2 mRNA containing-RAMs were incubated with C2C12-BRE/Luc cells, a stable cell line containing a BMP-response element fused with firefly luciferase reporter gene [31] (Fig. 6C), and the luciferase activity was monitored over time (Fig. 6D). Four experimental groups were set for comparison, *i.e.* RAM containing BMP2 mRNA (RAM-BMP2), RAM containing BMP2/NS1 mRNAs (RAM-BMP2/NS1), LPRs containing either BMP2 mRNA (BMP2) or BMP2/NS1 mRNAs (BMP2/NS1) (Fig. 6D). Maximal luciferase expression was observed 24 h post-transfection in the presence of freshly prepared LPRs (both BMP2 and BMP2/NS1 groups) and luciferase activity gradually decreased over time until 168 h (7 days). In contrast, in the presence of RAMs (both RAM-BMP2 and RAM-BMP2/NS1), the kinetics curve showed a peak of luciferase expression at later time, *i.e.* after 72 h of incubation; although decreasing over time, a noticeable luciferase activity was measured until 336 h (14 days) post-incubation. As a result, RAMs promoted luciferase expression for a duration of 2-fold longer than with fresh LPRs. More interestingly, the combination NS1 mRNA with BMP2 mRNA (either in LPR groups or in RAM groups) significantly enhanced the luciferase activity: the areas under the curve (AUC) for BMP2/NS1 and RAM-BMP2/NS1 were 2.4- and 3-fold higher than the ones obtained with BMP2 and RAM-BMP2/NS1 groups, respectively. These observations are consistent with our previous findings related to the beneficial effect of NS1 mRNA [22].

3.6. *RAM-BMP2/NS1 induces de novo bone formation in vivo*

RAM-BMP2, RAM-BMP2/NS1 and CoLL-1nHA scaffolds were implanted subcutaneously into the mice back for 8 weeks. Following surgical retrieval, there was no evidence of inflammation or rejection around any scaffold; RAM-BMP2/NS1 explants were also found to be well vascularized (Fig. 7A). Specimens were examined for micro-CT and histological analyses. Representative micro-CT images and quantification of the new bone tissue from these images are shown in Fig. 8. No bone deposit was found in CoLL-1nHA scaffolds proving that these matrices were not osteoinductive *per se*. Whereas a minimal bone tissue was observed in some RAM-BMP2 scaffolds, bone deposits were observed in 7 out of 8 RAM-BMP2/NS1 samples (Fig. 7B). In four of them, the bone tissue is surrounded the scaffold as a thin peripheral shell connected with internal trabeculae. Quantification of the bone using μCT-analysis confirmed significantly (2.1-fold) enhanced bone formation when BMP2 mRNA was co-delivered with NS1 (Fig. 7C).

Histological examination of the explants was consistent with

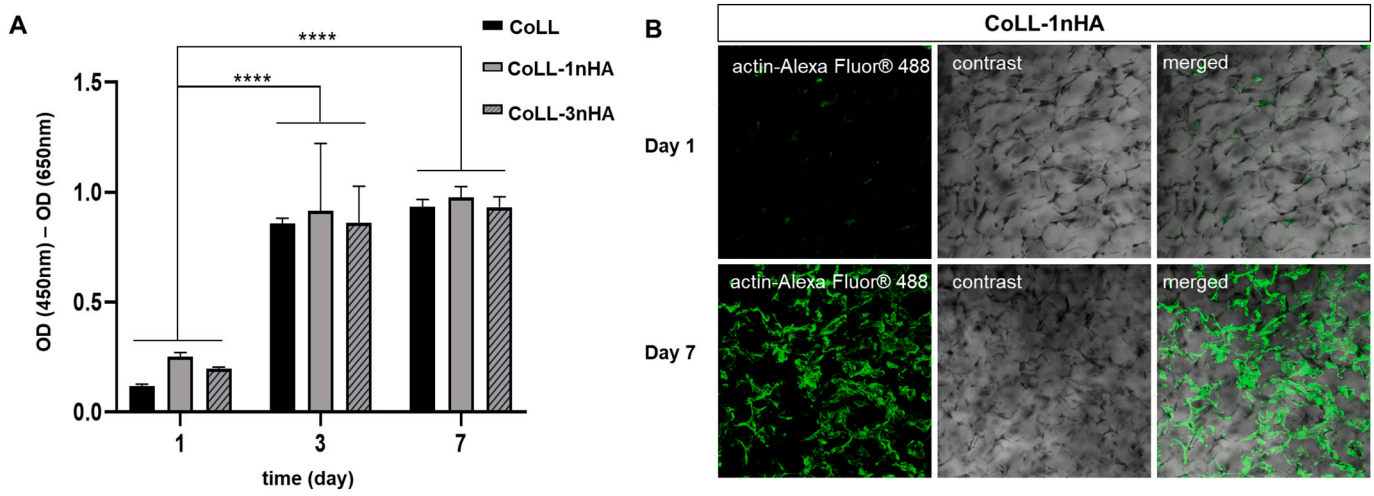

Fig. 4. Cell proliferation in collagen and collagen-nanohydroxyapatite scaffolds. C2C12 cells were seeded into the CoLL, CoLL-1nHA and CoLL-3nHA scaffold, respectively. (A) Day 1, day 3, and day 7 post-seeding, cell growth in each scaffold was measured *via* XTT assay. 2way ANOVA, Tukey's multiple comparisons test, was used for statistical analysis. (B) Confocal laser scanning microscopy images of CoLL-1nHA-C2C12 constructs after being cultured for 1 and 7 days. Actin was labeled with anti-actin antibody and Alexa Fluor® 488-conjugated secondary antibody. Images were obtained with 10 x microscope objective.

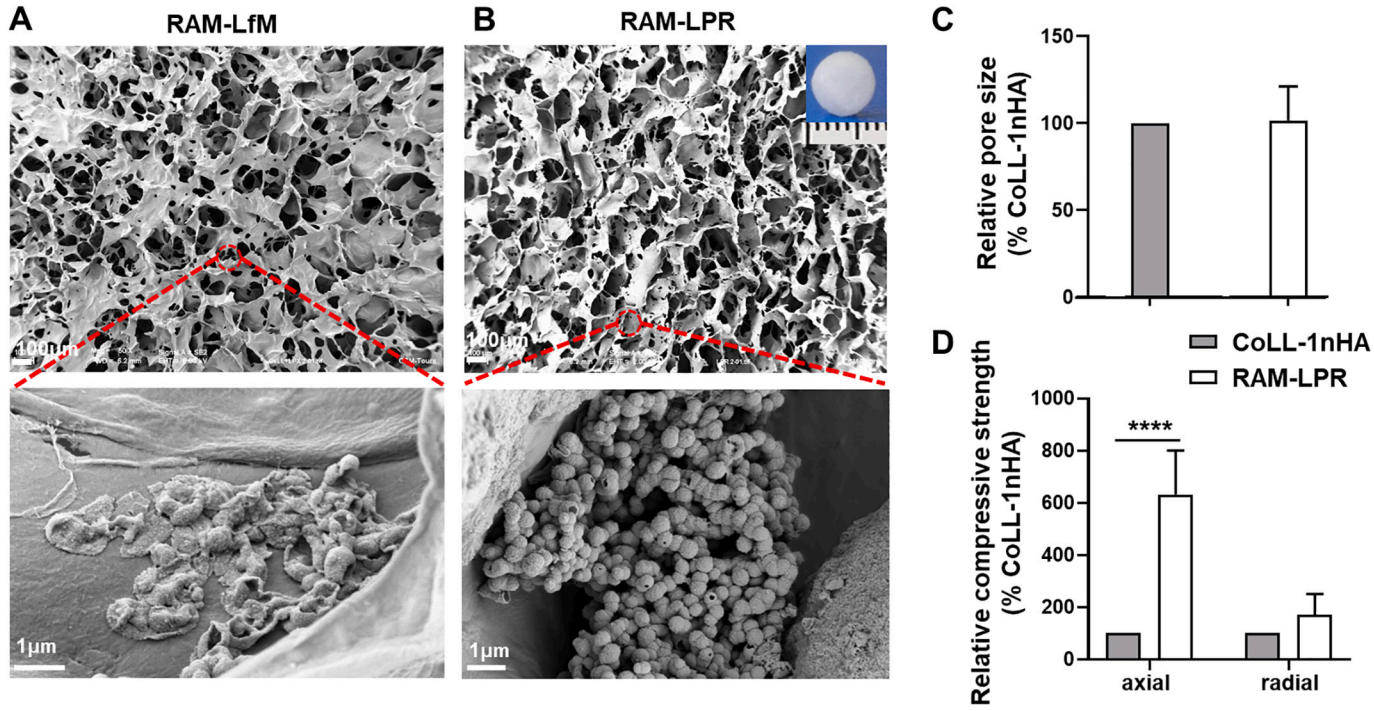

Fig. 5. Characterization of RAMs. The RAMs were prepared based on CoLL-1nHA scaffold by loading with LfM/mRNA complexes (RAM-LfM) or with LPRs (RAM-LPR). (A, B) Representative SEM images of RAMs (upper) with magnifications corresponding to vector/mRNA complexes (lower). B-insert shows a photograph of RAM-LPR. (C) Relative pore sizes of RAM-LPR calculated from SEM images, and normalized to the mean pore size of CoLL-1nHA ($n = 8$). (D) The axial and radial compressive strengths of RAM-LPR normalized to the mean compressive strengths of CoLL-1nHA ($n = 4$). Multiple *t*-tests was used for statistical analysis.

radiographic findings. Representative gross view of CoLL-1nHA controls confirmed absence of bone tissue and revealed a substantial colonization of the scaffold with fibrous tissue, but only peripheral (< 500 mm of depth) (Fig. 8A and D), the center of the scaffold remained acellular (Fig. 8E). RAM-BMP2 matrices were entirely colonized with highly vascularized fibrous tissue and minimal bone tissue was observed at the periphery of the scaffold (Fig. 8 B, G, F). The Masson's Trichrome staining, which identifies bone and osteoid matrix, revealed the large bony ossicles induced by RAM-BMP2/NS1. The bone tissue was organized as thin and mature bone trabeculae present mainly at the outer part of the implants and forming a shell (Fig. 8C, H); the center of the ossicles was occupied by bone marrow, containing numerous adipocytes, and by dense fibrous tissue (Fig. 8I). Additionally, Tartrate Resistant Acid Phosphatase (TRAP) staining, which reveals the presence of osteoclasts or osteoclast-like multinucleated giant cells (MNGC), was found either on the bone surfaces (Fig. 8L) or in soft tissue close to the bone tissue (Fig. 8K, L), indicating some extent of osteoclastic activity and, therefore, of bone remodeling activity.

4. Discussion

These last years, the delivery of mRNA for therapeutic purposes has

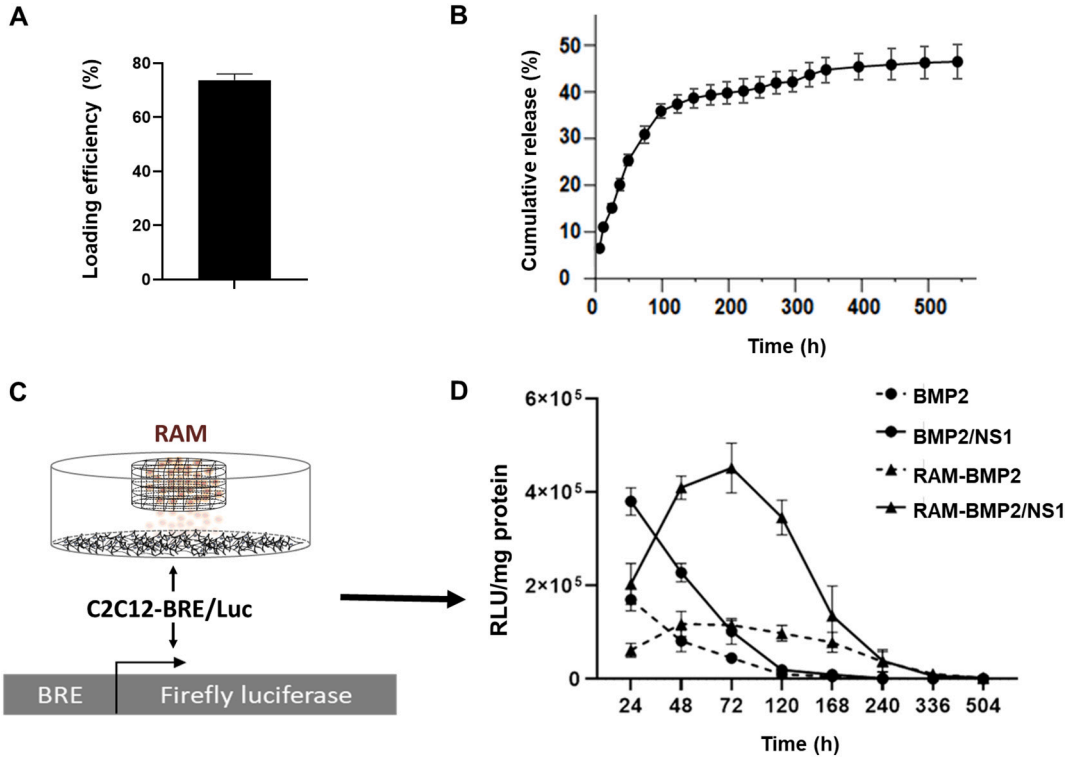

Fig. 6. LPRs release and activity. (A, B) The loading and release kinetics of LPRs from RAM containing 20 μg mRNA. RAMs were incubated in TE buffer at 37 °C, and the released mRNA were quantified after labeling with RiboGreen™. (C, D) The transfection activity of released LPRs. The RAMs containing 20 μg BMP2 mRNA (RAM-BMP2) or 15 μg BMP2/ 5 μg NS1 mRNAs (RAM-BMP2/NS1) were incubated in wells containing cultured C2C12A-BRE/Luc cells that stably express luciferase under BMP-2 stimulation (BMP-2 responses element, BRE). 1 μg BMP2 mRNA (BMP2) and 0.75 μg BMP2/0.25 μg NS1 mRNA (BMP2/NS1), formulated as LPRs, were set as controls. At indicated time points, C2C12-BRE/Luc cells were harvested and lysed for luciferase expression assay. The statistic differences among the groups within each time point are shown in Supplementary Table 2.

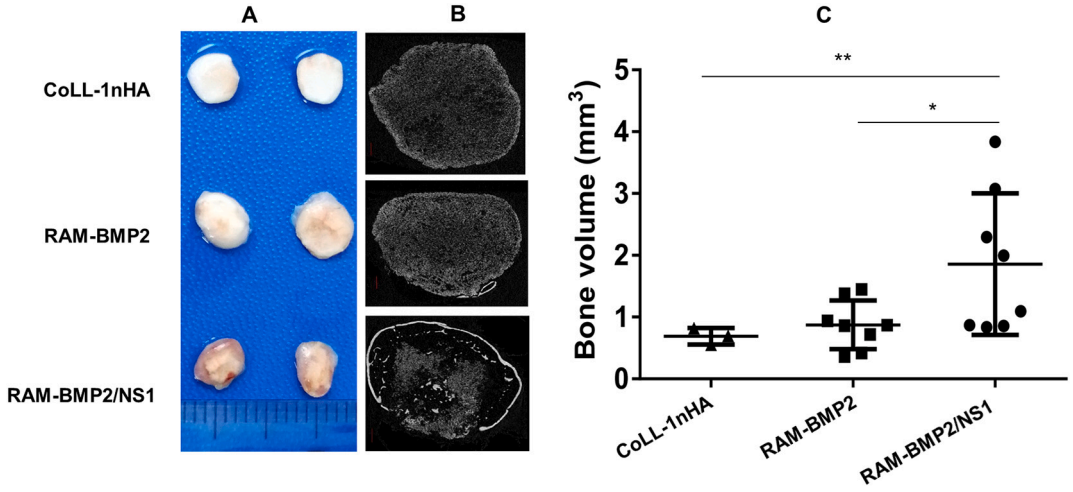

Fig. 7. Micro-CT analysis of bone induced by RAMs. (A) Representative photos of retrieved mRNA-free (CoLL-1nHA), BMP2 mRNA LPRs containing-RAM (RAM-BMP2) and BMP2/NS1 mRNAs LPRs containing-RAM (RAM-BMP2/NS1) scaffolds 8 weeks post subcutaneous implantation. (B) Representative 2D (left) and 3D (right) μCT images of the retrieved scaffolds. (C) Bone formation quantified using μCT analysis. $N = 3$ for CoLL-1nHA; $N = 8$ for RAMs. ANOVA with Dunnett's post-hoc test was used for statistical analysis.

gained remarkable progress [43], with extended application from vaccination to protein replacement therapies, such as cardiovascular regeneration [44]. The use of mRNA coding osteogenic proteins for bone regeneration is a field still in its infancy as it started from 2015 [14], and most of the studies are based on mRNA bearing modified nucleosides to improve their translatability [15–17]. Today, mRNA therapeutics are still costly due to the complex supply chain of their production including the addition of chemically modified nucleosides.

Unlike previously reported studies using chemically modified mRNA, here we report an alternative strategy using non-modified mRNAs to prepare bone graft substitutes, *i.e.* mRNA activated matrix (RAM), for *in vivo* osteoinduction. The mRNAs platform contains BMP2 mRNA and NS1 mRNA that works as an adjuvant to enhance BMP-2 expression by inhibiting host cell immune responses [22].

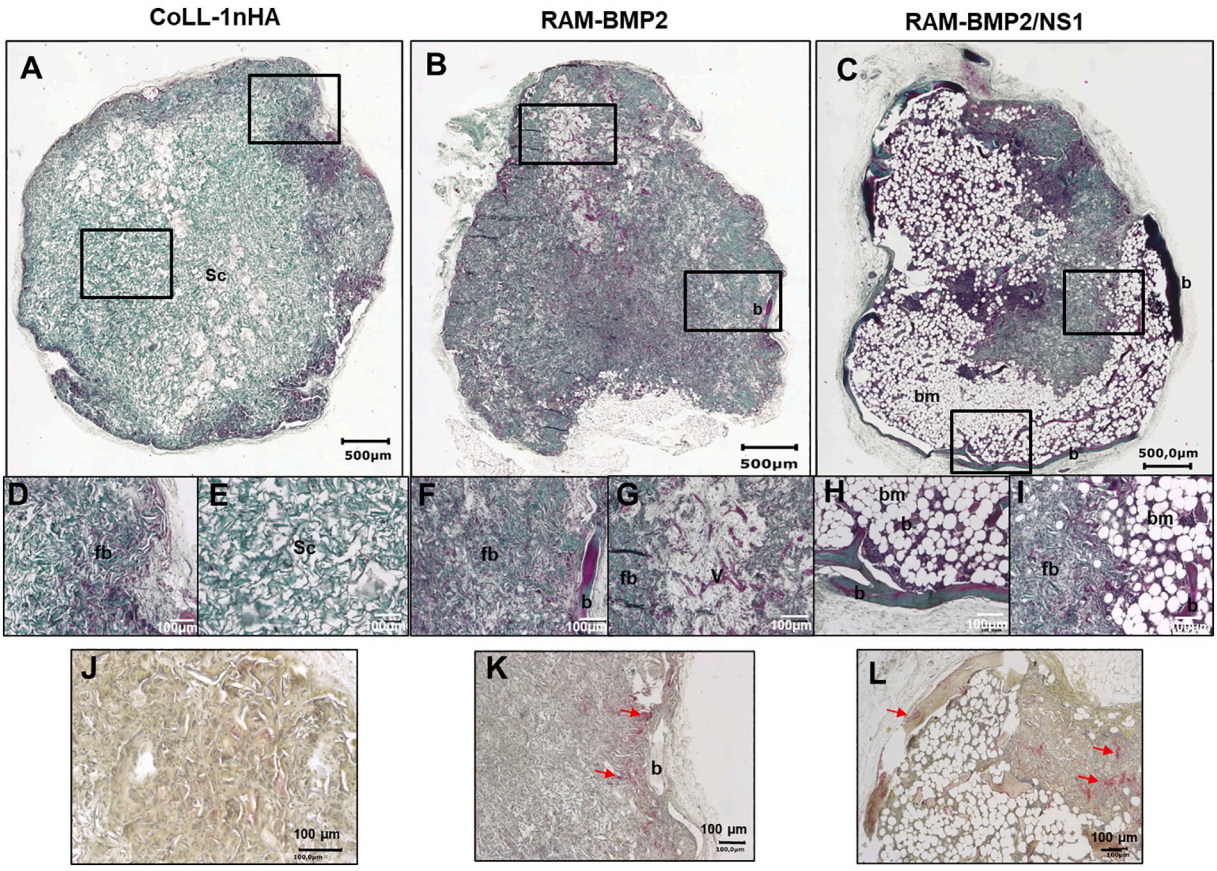

Fig. 8. Histology analysis of the explanted RAMs. The retrieved implants were demineralized, sliced and stained with either Masson's Trichrome (from A to I frames) or TRAP staining (from J to L frames). Representative sections of the (A-D-E) CoLL-1nHA, (B-F-G) RAM-BMP2 and (C-H-I) RAM-BMP2/NS1 scaffolds. For each scaffold, pictures from both outer or inner areas were shown at higher magnification. (J-K-L) TRAP staining revealed presence of osteoclastic activity. (Sc) Scaffold; (Fb) Fibrous tissue; (b) Bone tissue; (bm) fatty bone-marrow like tissue; (v) vessels; (red arrows) TRAP staining. (For interpretation of the references to colour in this figure legend, the reader is referred to the web version of this article.)

Our data shown in fig. 2 indicate that the optimal ratio of NS1 and BMP2 mRNAs determined for murine cells is also efficient for human cells. In line with our previous results, BMP2/NS1 mRNA transfected hMSCs yielded a significantly higher amount of BMP-2, than single BMP2 mRNA transfected cells. Interestingly, in those cells, the produced amount of BMP-2 from the dual mRNAs delivery was stable up to 60 h. As a result, one could expect to get a significant expression of osteogenic genes in the transfected hMSCs. However, no significant difference between the BMP2/NS1 group and BMP2 group was observed for most of the osteogenic genes and the deposited extracellular calcium. This phenomenon could be caused by two reasons. First, the transient expression profile of administered mRNA. After 3 days, the BMP2/NS1 group and BMP2 group had similar BMP-2 expression. In contrast, the MSCs osteogenic differentiation needs 2 weeks of continuous stimulation. Second, it has been reported that human derived MSCs have low responsiveness to BMPs [45,46]. Thus, although the BMP2/NS1 group resulted in significantly higher BMP-2 than the BMP2 group in the first 3 days, no significant difference was induced in gene level of osteoblastic markers (except for Runx2 at day 3). Despite those data, the significant enhanced production of BMP2 with the dual mRNAs delivery is encouraging and opens the room for improvement.

In clinical practice, bone grafts are critical for reconstructing massive bone loss or complex non-union defects [47]. According to a recent investigation from Zion market research, the global bone grafts and substitutes market was approximately $ 2745 million in 2018 and is expected to generate around $ 4235 million by 2026, registering a compound annual growth rate (CAGR) of 5.6% during the forecast period (accessed on 3rd January 2020). To meet this increasing demand, the aim of the BTE is to construct bone substitutes (BTE grafts) that as close as possible to the gold standard autografts through components, structure and function mimicking [1,48].

RAM have emerged as an advanced approach for constructing bone graft substitutes with the combination of BTE technology and mRNA-therapy technology [14,16].

Here, the collagen and nanohydroxyapatite (nHA), which represent the primary organic and inorganic compound in natural bone, were chosen to produce the basal porous scaffold. In preliminary experiments, we compared the type I collagen from bovine Achilles tendon and calf skin. As shown in S. Fig. 1, the bovine Achilles tendon collagen made scaffold exhibited closed pore structure which decreased its water absorption ability. The low pore interconnection will lead to less fluid exchange and cell invasion, and finally less or no new bone formation during *in vivo* application [40]. The likely explanation of this phenomenon is the solubility and fibrillar level differences between the two kinds of collagen. In Achilles tendon, the collagen fibers and fibrils are highly cross-linked and organized as parallel strands along the loading axis [49], which makes it acid-insoluble. In contrast, skin collagen fibrils, especially for young species, are less cross-linked and randomly distributed in the dermal layer of skin [50]. During scaffold preparation, the collagen from calf skin homogeneously dissolved in acetic acid solution resulting in continuous interpenetrating ice network after freezing, and forming interconnective porous structure after sublimation. While, the bovine Achilles tendon only swelled, even after three times longer incubating time. Thus, the calf skin collagen was selected as basal material for further combination with nHA.

As expected, the nHA reinforced collagen scaffold (CoLL-1nHA,

CoLL-3nHA) had an increased mechanical strength, especially in axial. During scaffolds freeze-drying, the aqueous solution was sublimated mainly through axial direction leading more pores aligned in the axial direction. It was reported that the mechanical properties of a porous scaffold depend on the direction of the loading along the pore channels [51]. More nHA in CoLL-3nHA decreased its interconnection degree (in terms of porosity). The elimination of micropores from the pore walls, and the non-embedded nHA, to some extent, resulted in its low porosity. Both the porosity, the permeability and the mechanical properties are crucial parameters for the BTE scaffold, influencing host cell ingrowth, migration and proliferation [1,40]. For instance, Lewandrowshi et al., found that the poly(propylene fumarate) scaffold has a higher porosity generating a greater and deeper bone ingrowth in rat tibias defect model [52] due to higher level of vascularization and fluid permeability [53].

In terms of biological performance, the addition of nHA did not show any significant influence on cell growth. Compared to CoLL and CoLL-3nHA, the CoLL-1nHA preserved slightly more cells, which could be caused by its high porosity, and the rough wall surface. This is in line with the study from Yuan et al., who showed that the surface roughness enhances the attachment, proliferation of anchorage-dependent bone forming cells [54].

To note, all scaffolds prepared in this study underwent chemically crosslinking (EDC: NHS: collagen carboxyl group molar ratio of 10: 4: 1), enabling them more resistance to enzyme degradation during *in vivo* usage (S. Fig. 2). In addition, the crosslinking resultant mechanical enhancement has been shown to increase osteoblast cell number and cellular distribution within collagen scaffolds [55]. Overall, the outstanding physical and biological performances of CoLL-1nHA giving it the valuable interesting candidate for preparing RAM.

IVT mRNA mediated immunogenicity and lacking of efficient *in vivo* delivery vector are the main obstacles relating to mRNA therapy application. By introducing NS1, we resolved the immunogenicity concerning. Next, we need a proper vector to deliver the therapeutic mRNAs to exert their function *in vivo*.

We previously reported a lipopolyplex (LPR) formulation to delivery small interfering RNA (siRNA) *in vitro* [24]. The Lip100/His-lPEI/siRNA formulated LPRs were more efficient than formulations made with commercial vectors, *i.e.* JetPRIME™, INTERFERin® and Lipofectamine™2000. The formulation was then transferred to this study to complex and deliver mRNA. During *in vitro* and *in vivo* transfection studies, LPRs showed a reversed trend compared to the commercial vector (Lipofectamine™ MessengerMax, LfM). We are not surprised by the results, as LfM is designed and optimized for *in vitro* cultured cell transfection, and LPRs for *in vivo* environment. Indeed, in our previous studies, although different in polymer and liposome, the LPRs formulation has been successfully used for *in vivo* vaccination, against tumors and influenza A virus [25,30].

On the other hand, from the aspect of surgical handling and cost of transport and storage, a ready-to-use RAM is more in line with market demand. After freeze-drying, within the RAM, the majority of LPR particles maintained a spherical shape, while LfM/mRNA particles collapsed, highly due to lack of supportive polyplex cores. The structure integrity helped the LPRs preserve their mRNA delivery ability. Compared to one-time transfection, the protein expression from the RAM groups was increased over 72 h prior to decrease. From the LPRs release profile, we conclude that this phenomenon could be generated by multiple transfections of cells thanks to continuously released LPRs.

Compared to the basal scaffold (CoLL-1nHA), the LPRs loading enhanced compressive strength, especially in the axial direction. The LPRs were prepared in HEPES buffer containing 5% sucrose, thus, after sublimation, the HEPES and sucrose molecules homogeneously deposit on pore walls, which may contribute to the mechanical changes as toughener.

The observed ectopic bone formation in mice induced by the BMP2 mRNA containing-matrices confirmed the osteoinductive performance of the RAM system. The co-delivery of NS1 mRNA with BMP2 mRNA significantly (2-fold) improved the potential of RAMs to promote new bone formation. The 3D μ-CT images and histology revealed that RAM-BMP2/NS1 induced large bony ossicles, typical of BMP-2-induced ectopic bone induction with the formation of a shell enclosing thin bone trabeculae and fatty bone marrow. The cells involved in the ectopic bone include both (i) cells that are transfected with the delivered mRNA and consequently produce and secrete the BMP-2 protein and (ii) cells that are activated by the paracrine BMP-2 and induce the bone matrix synthesis: Regarding the latter cells, it is reported that the ectopic bone formation mediated by BMP-2 results from osteogenic differentiation of circulating mesenchymal precursor cells (including myoblast [56] and adipocyte [57,58] progenitors and pericytes [59]), which are locally exposed to the growth factor; For the former cells, they may be the same as the latter ones (*i.e.* recruited local osteoprogenitors) or any other type of cells recruited within the scaffold, including inflammatory cells (monocytes /macrophages) or fibroblasts. The single delivery of BMP2 mRNA promoted minimal bone tissue which were entirely invaded by highly vascularized fibrous tissue. It is known that BMP-2 promotes bone formation in a dose-dependent manner [60]. At lower dose, BMP-2 did not induce bone formation, instead exert functions of cell chemotaxis and angiogenesis [61,62]. In contrast to RAM-BMP2/NS1 and RAM-BMP2, CoLL-1nHA scaffolds prepared without mRNA paucity of bone tissue induction and were only peripherally invaded by host tissue.

Although, the subcutaneous ectopic model has the advantage of evaluating the "true" osteoinductive capability of constructs since osteogenesis and osteoconduction mediated by the bone bed of the recipient animal does not occur at this location, considering the therapeutic application, an *in-situ* bone defect repair study is in progress combining the advanced 3D printing technology to optimize the mRNA delivery matrix. We believe that, when applied in the osteoprogenitors enrich environment, the RAM-BMP2/NS1 can further exert its function and induce as higher new bone tissue as reported previously [14], and the osteoinductive mechanism will be assessed afterwards.

5. Conclusion

In this study, we demonstrated the non-modified dual mRNAs (BMP2/NS1 mRNAs) system was capable to substantially improve the production of BMP-2 when applied to hMSCs *in vitro*, however, leading to slightly enhancement in osteogenic commitment. The main results concern the use of Lip100/His-lPEI based LPR that can serve as an mRNA delivery formulation for the production of RAMs made with collagen-nanohydroxyapaptite scaffold. RAMs-BMP2/NS1 were able to mediate a high and prolonged *in vitro* BMP-2 expression and, excitingly, *in vivo* new bone induction. Taken together, these results provided the basis for translating this RAM-BMP2/NS1 matrix into *in vivo* bone defect intervention. Moreover, as an advanced combination of mRNA therapy and tissue engineering, the RAM technology has broad potential applications, such as for wound healing, skin, cartilage and vertebral disc regeneration.

Author contributions

Pichon C and Wang P conceptualized the idea; Pichon C and Logeart-Avramoglou D supervised the work; Wang P, Perche F, Cabral S.D. C, Malarda V and Hanane EI-Hafci performed the experiments and data analysis; Wang P wrote the original draft; Pichon C, Logeart-Avramoglou D, Perche F, Correia J. I, Petite H and Patrick Midoux reviewed and edited the draft.

Data availability

The raw data required to reproduce these findings are available on request.

Acknowledgment

We are grateful to David Gosset from the P@CYFIC platform (CBM) for technical help in confocal laser scanning microscopy observation, Antony Delalande and Cyril Guimpied for mice surgery assistance, and Audrey Sauldubois from the Centre de Microscopie Electronique platform (Université d'Orléans) for TEM study. We also thank Sonia Georgeault from Plateforme IBiSA de Microscopie Electronique de l'Université de Tours for SEM observation. Region Centre Val de Loire and CNRS supported this work. Pinpin Wang was supported by a CSC grant from China.

Appendix A. Supplementary data

Supplementary data to this article can be found online at https://doi.org/10.1016/j.jconrel.2021.04.021.

References

[1] A.R. Amini, C.T. Laurencin, S.P. Nukavarapu, Bone tissue engineering: recent advances and challenges, Crit. Rev. Biomed. Eng. 40 (5) (2012) 363–408.
[2] V. Campana, G. Milano, E. Pagano, M. Barba, C. Cicione, G. Salonna, W. Lattanzi, G. Logroscino, Bone substitutes in orthopaedic surgery: from basic science to clinical practice, Journal of materials science. Materials in medicine 25 (10) (2014) 2445–2461.
[3] R.J. O'Keefe, J. Mao, Bone tissue engineering and regeneration: from discovery to the clinic–an overview, Tissue Eng Part B Rev 17 (6) (2011) 389–392.
[4] X. Zhai, C. Ruan, Y. Ma, D. Cheng, M. Wu, W. Liu, X. Zhao, H. Pan, W.W. Lu, 3D-bioprinted osteoblast-laden nanocomposite hydrogel constructs with induced microenvironments promote cell viability, differentiation, and osteogenesis both in vitro and in vivo, Adv Sci (Weinh) 5 (3) (2018) 1700550.
[5] S. D'Mello, K. Atluri, S.M. Geary, L. Hong, S. Elangovan, A.K. Salem, Bone regeneration using gene-activated matrices, AAPS J. 19 (1) (2017) 43–53.
[6] J. Fang, Y.Y. Zhu, E. Smiley, J. Bonadio, J.P. Rouleau, S.A. Goldstein, L. K. McCauley, B.L. Davidson, B.J. Roessler, Stimulation of new bone formation by direct transfer of osteogenic plasmid genes, Proc. Natl. Acad. Sci. U. S. A. 93 (12) (1996) 5753–5758.
[7] I. Ono, T. Yamashita, H.Y. Jin, Y. Ito, H. Hamada, Y. Akasaka, M. Nakasu, T. Ogawa, K. Jimbow, Combination of porous hydroxyapatite and cationic liposomes as a vector for BMP-2 gene therapy, Biomaterials 25 (19) (2004) 4709–4718.
[8] H. Ito, M. Koefoed, P. Tiyapatanaputi, K. Gromov, J.J. Goater, J. Carmouche, X. Zhang, P.T. Rubery, J. Rabinowitz, R.J. Samulski, Remodeling of cortical bone allografts mediated by adherent rAAV-RANKL and VEGF gene therapy, Nat. Med. 11 (3) (2005) 291.
[9] P.-C. Chang, J.A. Cirelli, Q. Jin, Y.-J. Seol, J.V. Sugai, N.J. D'Silva, T.E. Danciu, L. A. Chandler, B.A. Sosnowski, W.V. Giannobile, Adenovirus encoding human platelet-derived growth factor-B delivered to alveolar bone defects exhibits safety and biodistribution profiles favorable for clinical use, Hum. Gene Ther. 20 (5) (2009) 486–496.
[10] M. Keeney, J.J. van den Beucken, P.M. van der Kraan, J.A. Jansen, A. Pandit, The ability of a collagen/calcium phosphate scaffold to act as its own vector for gene delivery and to promote bone formation via transfection with VEGF165, Biomaterials 31 (10) (2010) 2893–2902.
[11] S. Elangovan, S.R. D'Mello, L. Hong, R.D. Ross, C. Allamargot, D.V. Dawson, C. M. Stanford, G.K. Johnson, D.R. Sumner, A.K. Salem, The enhancement of bone regeneration by gene activated matrix encoding for platelet derived growth factor, Biomaterials 35 (2) (2014) 737–747.
[12] P. Wang, F. Perche, D. Logeart-Avramoglou, C. Pichon, RNA-based therapy for osteogenesis, Int. J. Pharm. 569 (2019) 118594.
[13] Z.S. Badieyan, T. Evans, Concise review: application of chemically modified mRNA in cell fate conversion and tissue engineering, Stem Cells Transl. Med. 8 (8) (2019) 833–843.
[14] S. Elangovan, B. Khorsand, A.V. Do, L. Hong, A. Dewerth, M. Kormann, R.D. Ross, D.R. Sumner, C. Allamargot, A.K. Salem, Chemically modified RNA activated matrices enhance bone regeneration, J. Control. Release 218 (2015) 22–28.
[15] B. Khorsand, S. Elangovan, L. Hong, A. Dewerth, M.S. Kormann, A.K. Salem, A comparative study of the bone regenerative effect of chemically modified RNA encoding BMP-2 or BMP-9, AAPS J. 19 (2) (2017) 438–446.
[16] E.R. Balmayor, J.P. Geiger, M.K. Aneja, T. Berezhanskyy, M. Utzinger, O. Mykhaylyk, C. Rudolph, C. Plank, Chemically modified RNA induces osteogenesis of stem cells and human tissue explants as well as accelerates bone healing in rats, Biomaterials 87 (2016) 131–146.
[17] W. Zhang, R.E. De La Vega, M.J. Coenen, S.A. Muller, C.J. Peniche Silva, M. K. Aneja, C. Plank, M. van Griensven, C.H. Evans, E.R. Balmayor, An improved, chemically modified RNA encoding BMP-2 enhances osteogenesis in vitro and in vivo, Tissue Eng. A 25 (1-2) (2019) 131–144.
[18] K. Kariko, M. Buckstein, H. Ni, D. Weissman, Suppression of RNA recognition by toll-like receptors: the impact of nucleoside modification and the evolutionary origin of RNA, Immunity 23 (2) (2005) 165–175.
[19] S. Uchida, K. Kataoka, K. Itaka, Screening of mRNA chemical modification to maximize protein expression with reduced immunogenicity, Pharmaceutics 7 (3) (2015) 137–151.
[20] B.G. Hale, R.E. Randall, J. Ortin, D. Jackson, The multifunctional NS1 protein of influenza a viruses, J Gen Virol 89 (Pt 10) (2008) 2359–2376.
[21] K.K.L. Phua, Y. Liu, S.H. Sim, Non-linear enhancement of mRNA delivery efficiencies by influenza a derived NS1 protein engendering host gene inhibition property, Biomaterials 133 (2017) 29–36.
[22] P. Wang, D. Logeart-Avramoglou, H. Petite, C. Goncalves, P. Midoux, F. Perche, C. Pichon, Co-delivery of NS1 and BMP2 mRNAs to murine pluripotent stem cells leads to enhanced BMP-2 expression and osteogenic differentiation, Acta Biomater. 108 (2020) 337–346.
[23] P.S. Kowalski, A. Rudra, L. Miao, D.G. Anderson, Delivering the messenger: advances in technologies for therapeutic mRNA delivery, Mol. Ther. 27 (4) (2019) 710–728.
[24] C. Gonçalves, M. Berchel, M.-P. Gosselin, V. Malard, H. Cheradame, P.-A. Jaffrès, P. Guégan, C. Pichon, P. Midoux, Lipopolyplexes comprising imidazole/imidazolium lipophosphoramidate, histidinylated polyethyleneimine and siRNA as efficient formulation for siRNA transfection, Int. J. Pharm. 460 (1–2) (2014) 264–272.
[25] K. Van der Jeught, S. De Koker, L. Bialkowski, C. Heirman, P. Tjok Joe, F. Perche, S. Maenhout, S. Bevers, K. Broos, K. Deswarte, V. Malard, H. Hammad, P. Baril, T. Benvegnu, P.A. Jaffres, S.A.A. Kooijmans, R. Schiffelers, S. Lienenklaus, P. Midoux, C. Pichon, K. Breckpot, K. Thielemans, Dendritic cell targeting mRNA lipopolyplexes combine strong antitumor T-cell immunity with improved inflammatory safety, ACS Nano 12 (10) (2018) 9815–9829.
[26] M. Mevel, G. Breuzard, J.J. Yaouanc, J.C. Clement, P. Lehn, C. Pichon, P.A. Jaffres, P. Midoux, Synthesis and transfection activity of new cationic phosphoramidate lipids: high efficiency of an imidazolium derivative, Chembiochem 9 (9) (2008) 1462–1471.
[27] M. Mevel, C. Neveu, C. Goncalves, J.J. Yaouanc, C. Pichon, P.A. Jaffres, P. Midoux, Novel neutral imidazole-lipophosphoramides for transfection assays, Chemical communications (27) (2008) 3124–3126.
[28] E. Bertrand, C. Goncalves, L. Billiet, J.P. Gomez, C. Pichon, H. Cheradame, P. Midoux, P. Guegan, Histidinylated linear PEI: a new efficient non-toxic polymer for gene transfer, Chem. Commun. 47 (46) (2011) 12547–12549.
[29] P. Midoux, C. Pichon, J.J. Yaouanc, P.A. Jaffrès, Chemical vectors for gene delivery: a current review on polymers, peptides and lipids containing histidine or imidazole as nucleic acids carriers, Br. J. Pharmacol. 157 (2) (2009) 166–178.
[30] F. Perche, R. Clemencon, K. Schulze, T. Ebensen, C.A. Guzman, C. Pichon, Neutral Lipopolyplexes for in vivo delivery of conventional and replicative RNA vaccine, Mol Ther Nucleic Acids 17 (2019) 767–775.
[31] M.B.D. Logeart-Avramoglou, K. Oudina, P. Ten Dijke, H. Petite, An assay for the determination of biologically active bone morphogenetic proteins using cells transfected with an inhibitor of differentiation promoter-luciferase construct, Anal. Biochem. 349 (2006) 78–86.
[32] A.J. Friedenstein, S. Piatetzky II, K.V. Petrakova, Osteogenesis in transplants of bone marrow cells, J Embryol Exp Morphol 16 (3) (1966) 381–390.
[33] A. Moya, N. Larochette, M. Bourguignon, H. El-Hafci, E. Potier, H. Petite, D. Logeart-Avramoglou, Osteogenic potential of adipogenic predifferentiated human bone marrow-derived multipotent stromal cells for bone tissue-engineering, J. Tissue Eng. Regen. Med. 12 (3) (2018) e1511–e1524.
[34] F. Perche, T. Benvegnu, M. Berchel, L. Lebegue, C. Pichon, P.A. Jaffres, P. Midoux, Enhancement of dendritic cells transfection in vivo and of vaccination against B16F10 melanoma with mannosylated histidylated lipopolyplexes loaded with tumor antigen messenger RNA, Nanomedicine 7 (4) (2011) 445–453.
[35] C.-Y. Lin, F. Perche, M. Ikegami, S. Uchida, K. Kataoka, K. Itaka, Messenger RNA-based therapeutics for brain diseases: an animal study for augmenting clearance of beta-amyloid by intracerebral administration of neprilysin mRNA loaded in polyplex nanomicelles, J. Control. Release 235 (2016) 268–275.
[36] G.M. Cunniffe, G.R. Dickson, S. Partap, K.T. Stanton, F.J. O'Brien, Development and characterisation of a collagen nano-hydroxyapatite composite scaffold for bone tissue engineering, Journal of materials science. Materials in medicine 21 (8) (2010) 2293–2298.
[37] G.S. Offeddu, J.C. Ashworth, R.E. Cameron, M.L. Oyen, Multi-scale mechanical response of freeze-dried collagen scaffolds for tissue engineering applications, J. Mech. Behav. Biomed. Mater. 42 (2015) 19–25.
[38] L.H.H. Olde Damink, P.J. Dijkstra, M.J.A. van Luyn, P.B. van Wachem, P. Nieuwenhuis, J. Feijen, Cross-linking of dermal sheep collagen using a water-soluble carbodiimide, Biomaterials 17 (8) (1996) 765–773.
[39] M. Bartos, T. Suchy, R. Foltan, Note on the use of different approaches to determine the pore sizes of tissue engineering scaffolds: what do we measure? Biomed. Eng. Online 17 (1) (2018) 110.
[40] V. Karageorgiou, D. Kaplan, Porosity of 3D biomaterial scaffolds and osteogenesis, Biomaterials 26 (27) (2005) 5474–5491.
[41] R. Nazarov, H.J. Jin, D.L. Kaplan, Porous 3-D scaffolds from regenerated silk fibroin, Biomacromolecules 5 (3) (2004) 718–726.
[42] L.E. Monfoulet, P. Becquart, D. Marchat, K. Vandamme, M. Bourguignon, E. Pacard, V. Viateau, H. Petite, D. Logeart-Avramoglou, The pH in the microenvironment of human mesenchymal stem cells is a critical factor for optimal osteogenesis in tissue-engineered constructs, Tissue Eng. A 20 (13–14) (2014) 1827–1840.
[43] U. Sahin, K. Karikó, Ö. Türeci, mRNA-based therapeutics—developing a new class of drugs, Nat. Rev. Drug Discov. 13 (10) (2014) 759.
[44] L. Zangi, K.O. Lui, A. von Gise, Q. Ma, W. Ebina, L.M. Ptaszek, D. Später, H. Xu, M. Tabebordbar, R. Gorbatov, B. Sena, M. Nahrendorf, D.M. Briscoe, R.A. Li, A.

J. Wagers, D.J. Rossi, W.T. Pu, K.R. Chien, Modified mRNA directs the fate of heart progenitor cells and induces vascular regeneration after myocardial infarction, Nat. Biotechnol. 31 (10) (2013) 898–907.
[45] D.L. Diefenderfer, A.M. Osyczka, G.C. Reilly, P.S. Leboy, BMP responsiveness in human Mesenchymal stem cells, Connect. Tissue Res. 44 (1) (2003) 305–311.
[46] A.M. Osyczka, D.L. Diefenderfer, G. Bhargave, P.S. Leboy, Different effects of BMP-2 on marrow stromal cells from human and rat bone, Cells Tissues Organs 176 (1–3) (2004) 109–119.
[47] R.J. Mobbs, M. Maharaj, P.J. Rao, Clinical outcomes and fusion rates following anterior lumbar interbody fusion with bone graft substitute i-FACTOR, an anorganic bone matrix/P-15 composite, Journal of neurosurgery. Spine 21 (6) (2014) 867–876.
[48] V. Kesireddy, F.K. Kasper, Approaches for building bioactive elements into synthetic scaffolds for bone tissue engineering, J. Mater. Chem. B 4 (42) (2016) 6773–6786.
[49] H. Khayyeri, P. Blomgran, M. Hammerman, M.J. Turunen, A. Lowgren, M. Guizar-Sicairos, P. Aspenberg, H. Isaksson, Achilles tendon compositional and structural properties are altered after unloading by botox, Sci. Rep. 7 (1) (2017) 13067.
[50] M. Yamauchi, D.T. Woodley, G.L. Mechanic, Aging and cross-linking of skin collagen, Biochem. Biophys. Res. Commun. 152 (2) (1988) 898–903.
[51] M. Mao, Y. Tang, K. Zhao, Z. Duan, C. Wu, Fabrication of porous titanium scaffolds with centrosymmetric pore channels and improved radial fracture loading, J. Mater. Sci. 54 (4) (2019) 3527–3535.
[52] K.U. Lewandrowski, J.D. Gresser, S. Bondre, A.E. Silva, D.L. Wise, D.J. Trantolo, Developing porosity of poly(propylene glycol-co-fumaric acid) bone graft substitutes and the effect on osteointegration: a preliminary histology study in rats, Journal of biomaterials science. Polymer edition 11 (8) (2000) 879–889.
[53] M. Mastrogiacomo, S. Scaglione, R. Martinetti, L. Dolcini, F. Beltrame, R. Cancedda, R. Quarto, Role of scaffold internal structure on in vivo bone formation in macroporous calcium phosphate bioceramics, Biomaterials 27 (17) (2006) 3230–3237.
[54] H. Yuan, K. Kurashina, J.D. de Bruijn, Y. Li, K. De Groot, X. Zhang, A preliminary study on osteoinduction of two kinds of calcium phosphate ceramics, Biomaterials 20 (19) (1999) 1799–1806.
[55] M.G. Haugh, C.M. Murphy, R.C. McKiernan, C. Altenbuchner, F.J. O'Brien, Crosslinking and mechanical properties significantly influence cell attachment, proliferation, and migration within collagen glycosaminoglycan scaffolds, Tissue Eng. A 17 (9–10) (2011) 1201–1208.
[56] T. Katagiri, A. Yamaguchi, M. Komaki, E. Abe, N. Takahashi, T. Ikeda, V. Rosen, J. M. Wozney, A. Fujisawa-Sehara, T. Suda, Bone morphogenetic protein-2 converts the differentiation pathway of C2C12 myoblasts into the osteoblast lineage, J. Cell Biol. 127 (6 Pt 1) (1994) 1755–1766.
[57] D. Chen, X. Ji, M.A. Harris, J.Q. Feng, G. Karsenty, A.J. Celeste, V. Rosen, G. R. Mundy, S.E. Harris, Differential roles for bone morphogenetic protein (BMP) receptor type IB and IA in differentiation and specification of mesenchymal precursor cells to osteoblast and adipocyte lineages, J. Cell Biol. 142 (1) (1998) 295–305.
[58] A. Mehrkens, F. Saxer, S. Guven, W. Hoffmann, A.M. Muller, M. Jakob, F.E. Weber, I. Martin, A. Scherberich, Intraoperative engineering of osteogenic grafts combining freshly harvested, human adipose-derived cells and physiological doses of bone morphogenetic protein-2, Eur Cell Mater 24 (2012) 308–319.
[59] A.I. Caplan, All MSCs are pericytes? Cell Stem Cell 3 (3) (2008) 229–230.
[60] E.A. Wang, V. Rosen, J.S. D'Alessandro, M. Bauduy, P. Cordes, T. Harada, D. I. Israel, R.M. Hewick, K.M. Kerns, P. LaPan, et al., Recombinant human bone morphogenetic protein induces bone formation, Proc. Natl. Acad. Sci. U. S. A. 87 (6) (1990) 2220–2224.
[61] M. Lind, E.F. Eriksen, C. Bünger, Bone morphogenetic protein-2 but not bone morphogenetic protein-4 and -6 stimulates chemotactic migration of human osteoblasts, human marrow osteoblasts, and U2-OS cells, Bone 18 (1) (1996) 53–57.
[62] G. Finkenzeller, S. Hager, G.B. Stark, Effects of bone morphogenetic protein 2 on human umbilical vein endothelial cells, Microvasc. Res. 84 (1) (2012) 81–85.